PNAS RESEARCH ARTICLE | MEDICAL SCIENCES

Dual roles of β-arrestin 1 in mediating cell metabolism and proliferation in gastric cancer

Huan Yu[a], Man Wang[a], Ting Zhang[a], Lihua Cao[a], Zhongwu Li[b], Yang Du[a], Yanru Hai[a], Xiangyu Gao[c], Jiafu Ji[c,1], and Jianmin Wu[a,d,1]

Edited by Robert Lefkowitz, HHMI, Durham, NC; received December 23, 2021; accepted July 29, 2022

β-Arrestin 1 (ARRB1) has been recognized as a multifunctional adaptor protein in the last decade, beyond its original role in desensitizing G protein-coupled receptor signaling. Here, we identify that ARRB1 plays essential roles in mediating gastric cancer (GC) cell metabolism and proliferation, by combining cohort analysis and functional investigation using patient-derived preclinical models. Overexpression of ARRB1 was associated with poor outcome of GC patients and knockdown of ARRB1 impaired cell proliferation both ex vivo and in vivo. Intriguingly, ARRB1 depicted diverse subcellular localizations during a passage of organoid cultures (7 d) to exert dual functions. Further analysis revealed that nuclear ARRB1 binds with transcription factor E2F1 triggering up-regulation of proliferative genes, while cytoplasmic ARRB1 modulates metabolic flux by binding with the pyruvate kinase M2 isoform (PKM2) and hindering PKM2 tetramerization, which reduces pyruvate kinase activity and leads to cellular metabolism shifts from oxidative phosphorylation to aerobic glycolysis. As ARRB1 localization was shown mostly in the cytoplasm in human GC samples, therapeutic potential of the ARRB1–PKM2 axis was tested, and we found tumor proliferation could be attenuated by the PKM2 activator DASA-58, especially in ARRB1^{high} organoids. Together, the data in our study highlight a spatiotemporally dependent role of ARRB1 in mediating GC cell metabolism and proliferation and implies reactivating PKM2 may be a promising therapeutic strategy in a subset of GC patients.

ARRB1 | gastric cancer | metabolic reprogramming | cell proliferation | PKM2

ARRB1 (β-arrestin 1) was originally known as a negative regulator of G protein-coupled receptor (GPCR) signaling, by binding to the activated and phosphorylated form of GPCR, which leads to signal desensitization and receptor internalization. Beyond this classic role, ARRB1 has been gradually recognized as a multifunctional adaptor protein to bind with diverse interaction proteins, exerting divergent physiological functions (1, 2). In the cytoplasm, ARRB1 can scaffold signaling complexes to initiate waves of intracellular signaling, including activating MAPK pathways through ERK or other MAP kinases, and inhibiting NF-κB activity by interaction with IκBα, a protein that binds NF-κB and inhibits its nuclear translocation and subsequent activity (3–6). More recently, it has been appreciated that ARRB1 can translocate into the nucleus to regulate gene expression: for example, binding with transcription factor CREB and histone acetyltransferase p300 to enhance histone H4 acetylation and promote transcription of *p27* and *c-fos* (1, 7).

Emerging evidences indicated ARRB1 involvement in cancer proliferation, invasion, or metastasis through diverse mechanisms adapted for cancers with different tissue of origin, including cytoplasmic ARRB1 interactions to activate Akt signaling pathway in the liver (8) and colorectal cancers (9), and nuclear ARRB1 binding with transcription factor HIF1A in breast (10) and prostate cancers (11), while with E2F1 in lung cancer (12, 13). However, a tumor-suppressor role of ARRB1 has also been observed. Overexpression of ARRB1 inhibited the growth of human brain neuroblastoma cells through regulating p27 transcription in the nucleus (7), and inhibited the progression of T cell acute lymphoblastic leukemia cells and triple-negative breast cancer cells via ARRB1 binding partners in the cytoplasm (14, 15). These clues implied a controversial but possibly tissue type-specific roles of ARRB1 in cancer. In this study, we reveal a spatial heterogeneity of ARRB1 subcellular localization in different cancer types, as well as a temporal heterogeneity during a full passage of gastric cancer (GC) organoid cultures, which may partially account for the complicated roles of ARRB1 in cancer.

GC is the fifth most common cancer and the fourth most common cause of cancer death globally (16, 17), and the exact function of ARRB1 in GC remains elusive. Our cohort analysis implied a new role of ARRB1 in GC metabolic reprogramming. Altered cell metabolism is an essential hallmark of cancer and intertwined with other cancer hallmarks, including autonomous growth, escape from apoptosis, and immune evasion (18, 19), which provides a potential vulnerability for cancer treatment. Thus, understanding how ARRB1 helps rewire

Significance

β-Arrestin 1 (ARRB1) has been known as a key negative regulator of G protein-coupled receptor signaling. During the past decade, it has been recognized that ARRB1 also functions as a signal transducer in its own right, by acting as an adaptor protein for various signaling pathways. In this study, we report that ARRB1 plays essential roles in mediating gastric cancer cell metabolism and proliferation through binding with pyruvate kinase PKM2 and transcription factor E2F1, respectively, in distinct subcellular localizations by a time-dependent manner. Furthermore, the altered cell metabolism by the ARRB1–PKM2 axis could be reverted by the PKM2 activator DASA-58, providing an opportunity for therapeutic development to target metabolic vulnerability in gastric cancer cells.

Author affiliations: [a]Key Laboratory of Carcinogenesis and Translational Research (Ministry of Education), Center for Cancer Bioinformatics, Peking University Cancer Hospital & Institute, Beijing 100142, China; [b]Department of Pathology, Peking University Cancer Hospital & Institute, Beijing 100142, China; [c]Gastrointestinal Cancer Center, Peking University Cancer Hospital & Institute, Beijing 100142, China; and [d]Peking University International Cancer Institute, Peking University, Beijing 100191, China

Author contributions: H.Y., J.J., and J.W. designed research; H.Y., M.W., and T.Z. performed research; Z.L., X.G., and J.J. contributed new reagents/analytic tools; H.Y., L.C., Y.D., Y.H., and J.W. analyzed data; and H.Y. and J.W. wrote the paper.

The authors declare no competing interest.

This article is a PNAS Direct Submission.

[1]To whom correspondence may be addressed. Email: wujm@bjmu.edu.cn or jijiafu@hsc.pku.edu.cn.

This article contains supporting information online at http://www.pnas.org/lookup/suppl/doi:10.1073/pnas.2123231119/-/DCSupplemental

Published September 26, 2022.

the intrinsic metabolism of GC cells may provide cues for development of novel therapeutic strategies in GC.

Here, our results demonstrate that ARRB1 expression is up-regulated in GC tissue samples and associated with poor patient outcome. Knockdown of ARRB1 impairs cell proliferation in both ex vivo and in vivo systems. ARRB1 depicts diverse subcellular localizations during a passage of organoid cultures (7 d) to exert dual functions. Nuclear ARRB1 interaction with E2F1 up-regulates expression of proliferative genes, while cytoplasmic ARRB1 interaction with the pyruvate kinase M2 isoform (PKM2) leads to metabolic reprogramming by hindering PKM2 tetramerization to reduces its pyruvate kinase activity. Together, our results indicate that a temporal and spatial regulation of ARRB1 orchestrates divergent routes to promote GC progression.

Results

ARRB1 Overexpression in GC Associated with Poor Prognosis. To understand the clinical implications of ARRB1, the expressions of ARRB1 in 171 paraffin-embedded GC specimens and 54 paired normal specimens were investigated by immunohistochemical (IHC) staining, which showed overall stronger intensity in tumor tissue (Fig. 1*A*). Furthermore, GC patients were divided into $ARRB1^{-}$, borderline, and $ARRB1^{+}$ groups based on IHC scores of tumor tissues (representative images shown in Fig. 1*B*). The $ARRB1^{+}$ group of GC patients showed significantly worse survival than the $ARRB1^{-}$ group ($P = 0.0038$), but there was no significant difference between the borderline and $ARRB1^{-}$ groups (Fig. 1*C*). Moreover, the $ARRB1^{+}$ group was enriched with diffuse GC patients ($P = 0.028$) and with a trend of enrichment in poorly differential patients ($P = 0.069$) (Dataset S1). The same survival association was also found between the $ARRB1^{high}$ and $ARRB1^{low}$ groups in locally advanced GC patients (seventh edition American Joint Committee on Cancer clinical staging II-III), based on a published mass spectrometry (MS)-based proteomic dataset ($P = 0.0073$) (*SI Appendix*, Fig. S1) (20). These results suggested that high expression of ARRB1 could be associated with poor prognosis in patients with GC.

We also investigated the subcellular localization of ARRB1, and found that most GC samples with detected ARRB1 protein expression depicted cytoplasmic localization (Fig. 1*D*). In contrast, a majority of normal tissues showed weak nuclear staining of ARRB1. This difference in expression and subcellular localization distribution might be associated with ARRB1 function in malignant transformation and progression. A recent study showed that about 50% of prostate cancer samples depicted ARRB1 nuclear localization (11), indicating a heterogeneity of ARRB1 subcellular localization in different tumor types.

Knockdown of ARRB1 Impairs GC Proliferation. To evaluate ARRB1 functions in GC, five patient-derived GC organoid lines (W065C, W066D, W066E, W070A, and W070B) were investigated. All organoids and their parental tissues have been previously profiled by whole-exome sequencing and RNA sequencing (RNA-seq), and organoids substantially recapitulated the genomic alterations of parental tissues. Among these five organoid lines, W070B and W066E depicted higher ARRB1 protein abundances, by both IHC staining (Fig. 2*A*) and Western blot analysis (Fig. 2*B*). Similar pattern of ARRB1 mRNA expression was shown using RNA-seq profiles (Fig. 2*C*).

Next, to determine the effect of ARRB1 on GC proliferation, we knocked down ARRB1 in all five organoid lines using two independent small-interfering RNAs (siRNAs) (*SI Appendix*, Fig. S2*A*). As shown by EdU staining, reduced expression of ARRB1 led to significantly decreased proliferation rates of organoids (Fig. 2*D*). Furthermore, two organoid lines with high ARRB1 expression (W070B and W066E) were selected for stable ARRB1 knockdown by short-hairpin RNA (shRNA), which achieved about 70% knockdown efficiency (Fig. 2*E*; transduction efficacy shown in *SI Appendix*, Fig. S3). The shARRB1 organoids-derived xenografts were also developed for in vivo investigation. Compared with non-targeting control (NTC) organoid lines, ARRB1 knockdown resulted in significant suppression of cell proliferation (Fig. 2*F*) and tumor formation (Fig. 2*G*), suggesting a proliferation-promoting role of ARRB1 in GC. For further verification, we conducted rescue experiments by reexpressing ARRB1 in shARRB1 organoids, and found that restoration of ARRB1 rescued the effects of ARRB1 knockdown on GC organoid proliferation (*SI Appendix*, Fig. S2*B*).

Subcellular Localization of ARRB1 Redistributed during a Passage of Organoid Cultures. During a passage of organoid cultures (7 d), we observed a change of ARRB1 subcellular localization at different time points. As shown by immunofluorescence staining, a substantial amount of ARRB1 translocated into the nucleus during days 1 to 3 after organoid passaging (a process starting from dissociating the organoids for regrowing), while mostly localized in the cytoplasm during days 4 to 7 (Fig. 3*A*). For validation, we performed subcellular fractionation of two organoid lines with high ARRB1 expression (W070B and W066E). A similar change of ARRB1 protein level was identified in the cytosolic and nuclear extracts by immunoblot analysis, with Tubulin and Lamin B used as control for preparation purity (Fig. 3*B*). This result was verified by two additional ARRB1 antibodies (*SI Appendix*, Fig. S4 *A*–*C*). Moreover, ARRB2 was found to be always localized in the cytoplasm (*SI Appendix*, Fig. S4*D*) as expected, as it was constitutively exported from the nucleus due to the nuclear export signal (NES) sequence at its C terminus, whereas no NES was in ARRB1 (3, 21).

Given its different subcellular distributions, we hypothesized that ARRB1 may participate in diverse underlying processes at different time points, as an adaptor protein to form different complexes with distinct functions. Thus, RNA-seq was applied to organoid cultures at days 1, 3, and 7 after passaging. Pathway enrichment analysis of significantly up-regulated genes at each time point (compared to all other time points) provided clues for the dysregulated biological processes (q value < 0.05) underlying the observed growth pattern of organoids. At day 1, organoids were dissociated into single cells or small fragments and seeded with a low density, and found with up-regulation of E2F targets and MYC targets (Fig. 3 *C*, *Left*). At day 3 postpassage, correlated with fast proliferation, K_i-67 achieved the highest level (*SI Appendix*, Fig. S5*A*) with up-regulation of G2M check point and mitotic spindle pathway genes (Fig. 3 *C*, *Center*). Subsequently, organoids gradually reached high density during days 4 to 7 (Fig. 3*A*), with metabolic pathway genes shown to be significantly dysregulated, including enrichment of up-regulated genes in hypoxia and glycolysis pathways (Fig. 3 *C*, *Right*) and down-regulated genes in the oxidative phosphorylation (OXPHOS) pathway (Dataset S2).

For further investigation, we removed epidermal growth factor (EGF), a key component of the tissue-specific growth factor mixture functioning as a mitogen stimulating organoid growth (22), from organoid culture medium at days 1 to 2 postpassage, to attenuate the proliferation signaling. We observed the impaired organoid growth (Fig. 3*D*), and the nuclear translocation of ARRB1 was also substantially attenuated after EGF removal (Fig. 3*E*), confirmed by immunoblot analysis of subcellular

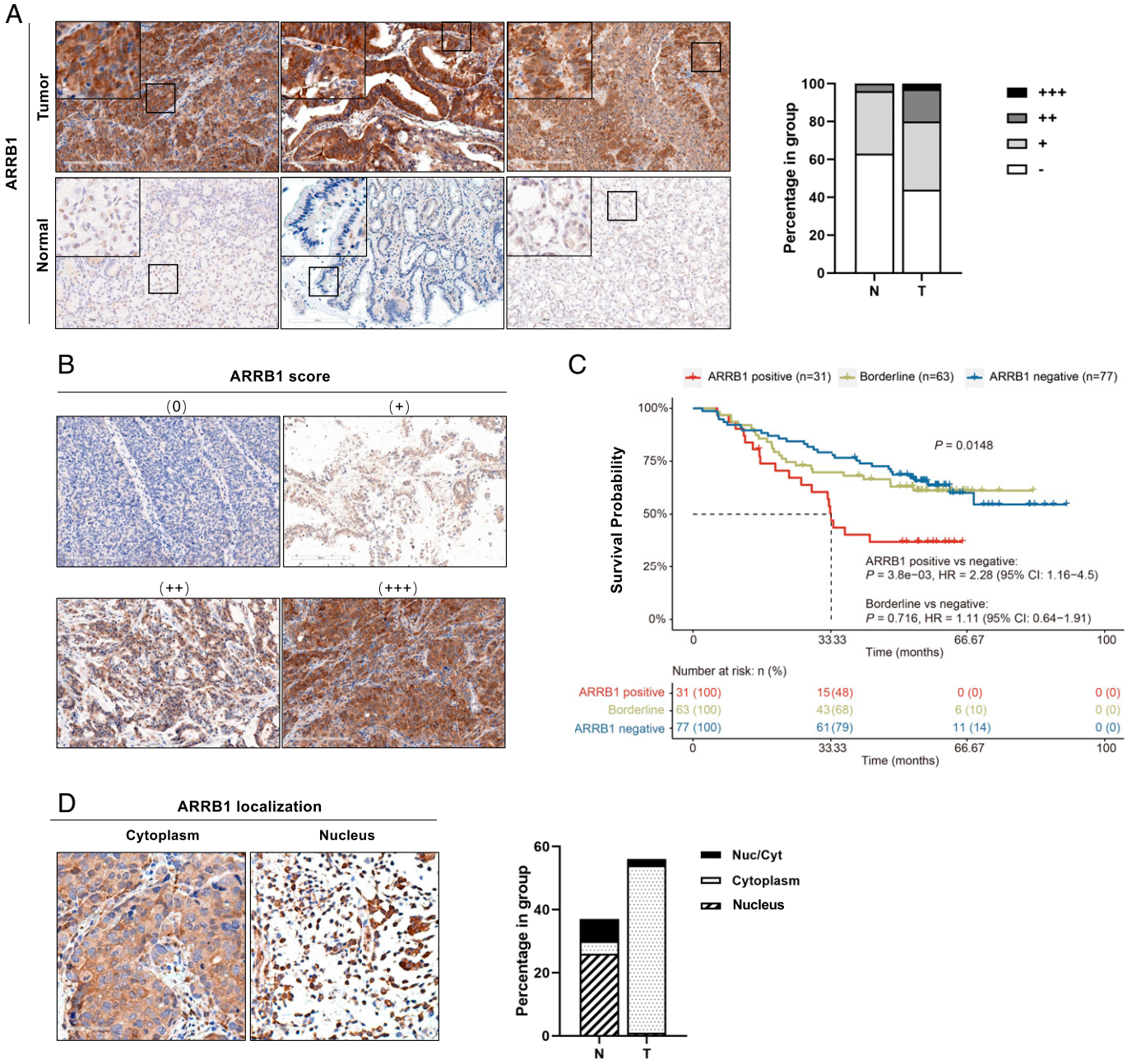

Fig. 1. Cytoplasmic ARRB1 elevated in GC and associated with poor prognosis. (*A*) Representative images of IHC staining of ARRB1 (*Left*), and stacked bar plots showing ARRB1 expression pattern in tumor and normal tissue (*Right*). (Scale bars, 200 μm.) Magnification at 10X. (*B*) Representative images of IHC staining of ARRB1 with different scores. (Scale bars, 200 μm.) Score 0 was regarded as ARRB1^{-}, while score 1+ as borderline, and score 2+ or 3+ as ARRB1^{+}. (*C*) Disease-specific survival curves of three groups of GC patients stratified by ARRB1 expression. *P* values were obtained using the log-rank test. (*D*) Representative images of cytoplasmic and nuclear staining of ARRB1 (*Left*) and stacked bar plots showing subcellular localization distribution of ARRB1 in the cohort (*Right*). (Scale bars, 60 μm.)

extracts (Fig. 3*F*). Together, these data implied a role of nuclear ARRB1 (nucARRB1) in EGF-induced tumor proliferation.

Furthermore, as E2F targets were significantly enriched in up-regulated genes at both day 1 (q value < 0.0001) and day 3 (q value < 10e-32) after passage (detailed information in Dataset S2), we investigated the link between ARRB1 and E2F1, a central transcription factor involved in cell cycle progression. Double-immunofluorescence results indicated that nucARRB1 colocalized with E2F1 (Fig. 3*G*), and immunoprecipitation analysis further confirmed an association of ARRB1 and E2F1 (using day 3 organoids) (Fig. 3*H*). This interaction was also reported in lung cancer (12, 13). Therefore, ARRB1 might act as a cofactor of E2F1, with an effect on E2F-induced gene expression.

Next, we tried to identify the potential proliferative genes coregulated by E2F1 and ARRB1. Based on RNA-seq profiles, known E2F target genes (from MSigDB v7.0) were analyzed to identify the ones with significant correlation with K_i-67 expression at day 1 and day 3 postpassage (Fig. 3*I*). The correlation analysis ($r > 0.2$ and $P < 0.05$, paired Pearson correlation test) identified 90 positively correlated E2F target genes, as potential E2F-mediated proliferative genes (*SI Appendix*, Fig. S5*B*). As ARRB1 expression was also strongly correlated with K_i-67 (P = 8.2e-05), we continued to identify the candidates with similar expression changes with ARRB1 in human GC samples. Using a published GC quantitative proteomic dataset (23), differential expression analysis identified two candidate E2F-mediated proliferative genes

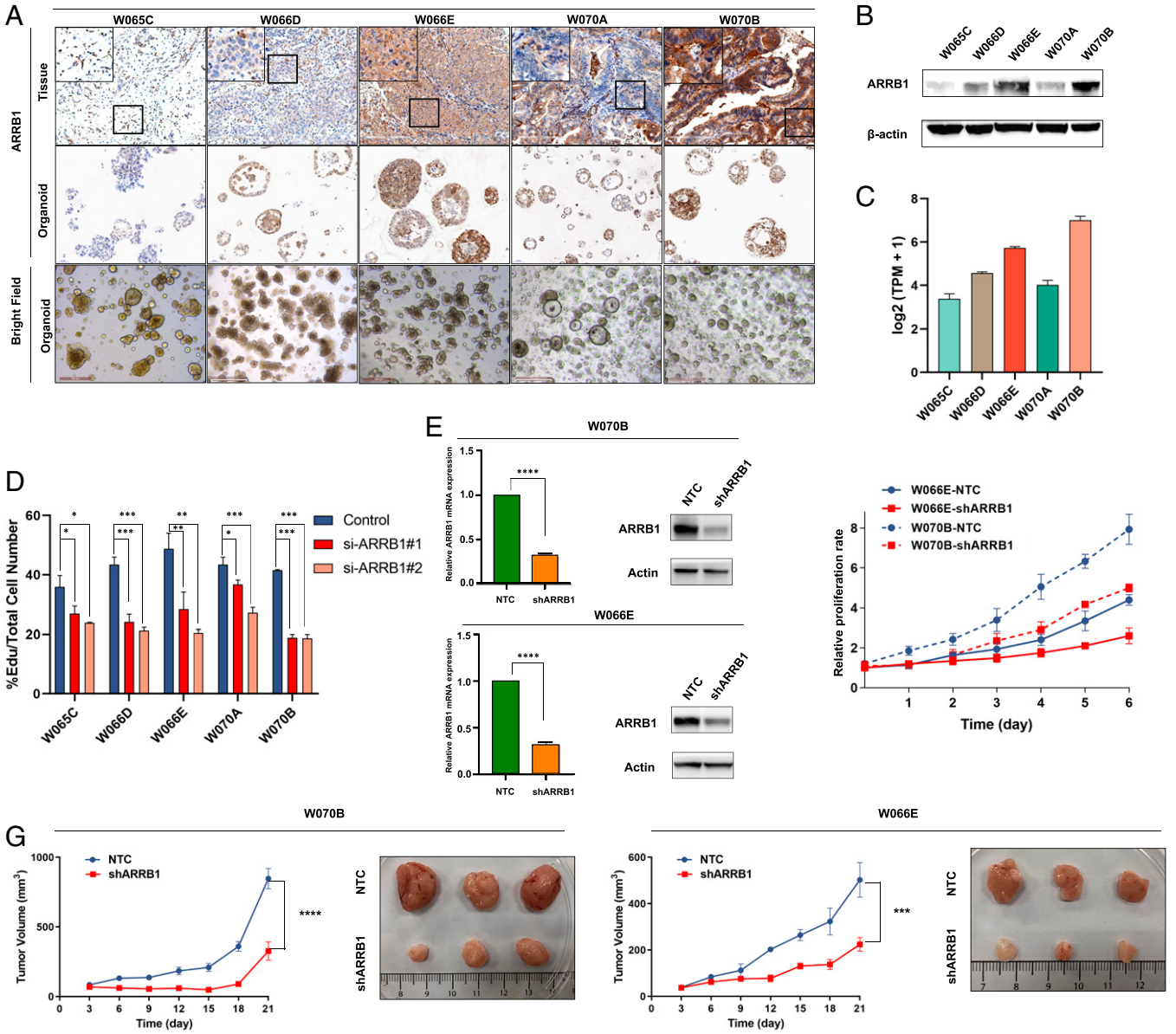

Fig. 2. Knockdown of ARRB1 inhibits GC proliferation. ARRB1 mRNA and protein levels in five GC organoid lines (*A*–*C*). (*A*, *Top* and *Middle*) Representative images of ARRB1 IHC staining in patient-derived organoids and the originating tumor tissue. (Scale bars, 50 μm, *Top*; 200 μm, *Middle*.) (*Bottom*) Representative images of brightfield organoids. (Scale bars, 500 μm.) (*B*) Western blots of ARRB1 in five organoid lines. (*C*) ARRB1 mRNA expression in five organoid lines based on RNA-seq profiles. (*D*) Proliferation rates of five organoid lines after siRNA-mediated ARRB1 knockdown, assessed by EdU proliferation assay. (*E*) The efficiency of shRNA-mediated ARRB1 knockdown in W066E and W070B organoids, evaluated by qPCR (*Left*) and Western blotting (*Right*). (*F*) Cell proliferation assays of shARRB1 W070B/W066E organoids compared to NTC (n = 3). (*G*) Growth curves of xenografts subcutaneously implanted with shARRB1 and NTC organoids (*Left*, n = 3), with the pictures of corresponding xenograft tumors (*Right*). P value computed using a two-sided Student's t test; $^{****}P < 0.0001$, $^{***}P < 0.001$, $^{**}P < 0.01$, $^{*}P < 0.05$.

(AURKA and KIF22) with significant up-regulation in ARRB1^{high} tumors (*SI Appendix*, Fig. S5*C*), implying a potential coregulation by ARRB1. Interestingly, both AURKA and KIF22 had microtubule-related functions during cell division with implications in cancer cell proliferation (24, 25), which warranted further investigation and validation. Together, our analyses indicated a proliferation promoting role of nucARRB1 in GC, which might be through association with E2F1.

ARRB1 Reprograms GC Cell Metabolism. As a high level of ARRB1 expression was shown at day 7, associated with dysregulation of metabolism-related pathway genes, the role of ARRB1 in GC metabolism was further explored in detail. We first evaluated whether elevated ARRB1 expression has an influence on the functional output of metabolic pathways. Glycolysis and mitochondrial respiration capacity were measured using extracellular media acidification rate (ECAR) and oxygen consumption rate (OCR) as surrogates, respectively. Among five organoid lines, organoids with higher ARRB1 expression depicted an increased rate of basal glycolysis and a decreased rate in basal mitochondrial respiration (Fig. 4 *A* and *B*). Moreover, ARRB1 knockdown significantly increased the ratio of OCR to ECAR in both W066E (Fig. 4 *C*–*E*) and W070B (Fig. 4 *F*–*H*) organoids, due to a consistent decrease in glycolysis, glycolytic capacity and glycolytic reserve (Fig. 4 *C* and *F*), along with an increase in basal mitochondrial respiration, maximal respiratory capacity, ATP production, spare respiration capacity, and proton leak (Fig. 4 *D* and *G*). Notably, the extent of influence by ARRB1 knockdown is more significant on glycolysis than mitochondrial respiration capacity. We

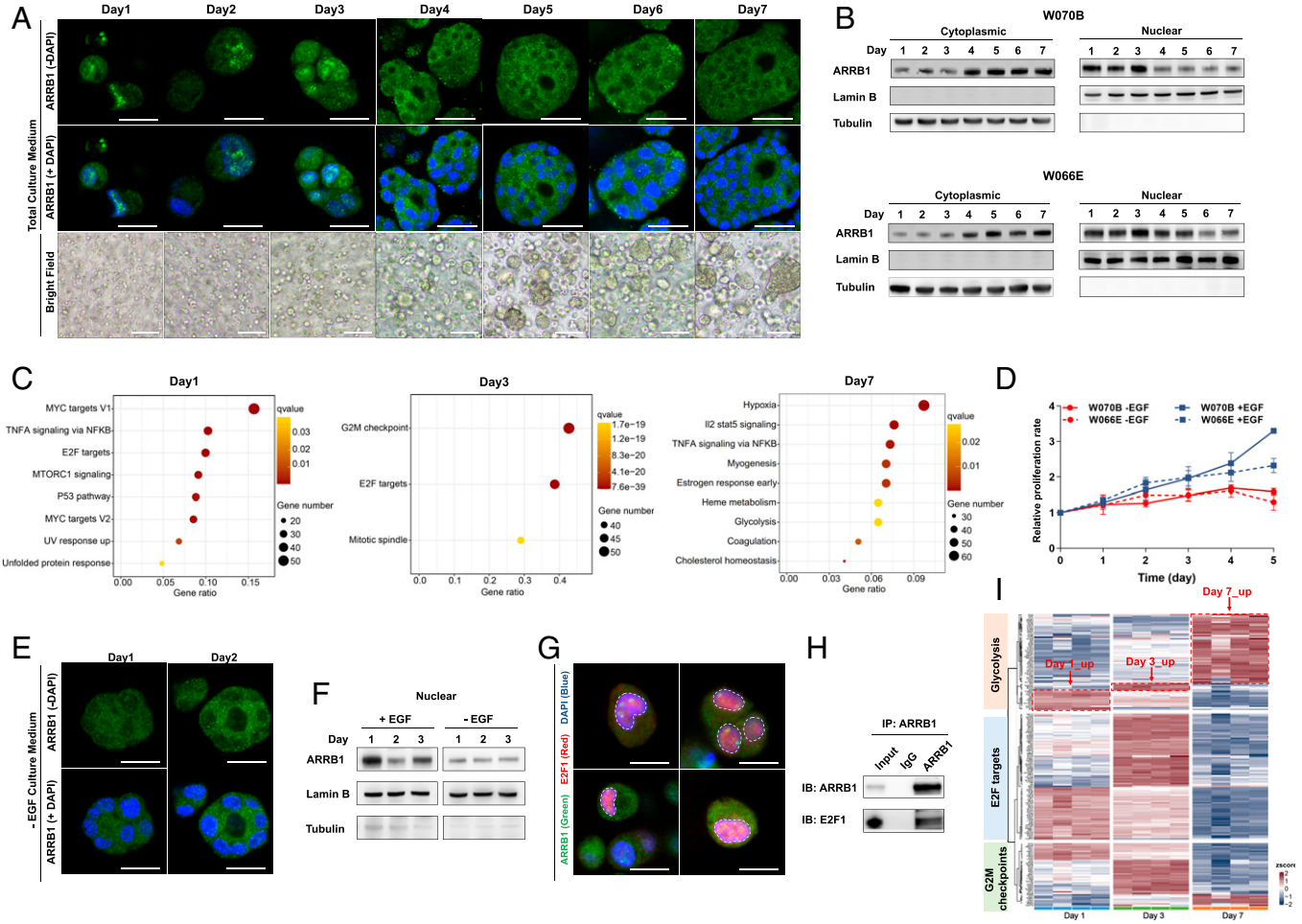

Fig. 3. Distinct subcellular localizations of ARRB1 at different proliferation time points. (*A*, *Top* and *Middle*) Immunofluorescence staining of ARRB1 (green) and DAPI (blue) at different time points after organoid passage (W070B). (The scale bars represents 25 μm in day 1 to 3 images and 50 μm in day 4 to 7 images.) (*Bottom*) Representative images of brightfield organoids. (Scale bars, 100 μm.) (*B*) Western blots of cytoplasmic and nuclear ARRB1 in W070B and W066E organoids, with Tubulin and Lamin B used as control for preparation purity. (*C*) Bubble plots showing enriched MSigDB HALLMARK gene sets (*q* value < 0.05) in up-regulated genes at days 1, 3, and 7 (compared to all other time points), respectively. Bubbles are colored according to false-discovery rate q-values, and the size of bubbles indicates the number of identified genes in a gene set. Gene sets were sorted by gene ratio. (*D*) Cell proliferation assays of W070B and W066E organoids, with and without EGF in the culture medium. (*E*) Immunofluorescent staining of ARRB1 (green) and DAPI (blue) at day 1 and day 2 after EGF withdrawal. (Scale bars, 25 μm.) (*F*) Western blots of nuclear ARRB1 at days 1, 2, and 3 before and after EGF withdrawal from culture medium. Lamin B served as loading control. (*G*) Immunofluorescent staining of ARRB1 (green), E2F1 (red), and DAPI (blue) at day 1 after organoid passage. Dotted lines mark nuclei of interest, in which yellow dots represent the subcellular localizations of ARRB1 and E2F1 interaction. (Scale bars, 25 μm.) (*H*) Immunoprecipitation assays performed with IgG and anti-ARRB1 antibodies in W070 organoids, followed by Western blotting analysis. (*I*) Heatmap showing row-scaled expression of glycolysis, E2F targets and G2M pathway genes up-regulated in at least one time point (days 1, 3, and 7). Up-regulated glycolysis pathway genes at each time point were indicated by dashed boxes with red border.

also investigated tissue respirometry in organoid-derived xenografts. Xenograft tumors with the highest ARRB1 level (W070B) depicted the greatest basal glycolysis capacity accordingly (*SI Appendix*, Fig. S6*A*), and consistently, shARRB1 organoids-derived xenografts (both W070B and W066E) showed significantly less basal glycolysis capacity than the corresponding NTC tumors (*SI Appendix*, Fig. S6 *B* and *C*).

We further performed nontargeted metabolomic profiling using ultraperformance liquid chromatography followed by tandem MS (UPLC-MS/MS), to investigate altered metabolites in ARRB1 knockdown organoids (W070B). Significant reductions in glycolysis intermediates (glucose, fructose, glucose-6-phosphate, fructose-6-phosphate, ribose-5-phosphate, lactate) and increases in TCA cycle intermediates (pyruvic acid, malic acid, fumaric acid, succinic acid, citric acid, *cis*-Aconitic acid, and oxoglutaric acid) were identified in shARRB1 organoids. Of note, multiple altered metabolites, including fructose-6-phosphate, glucose-6-phosphate, and ribose-5-phosphate, play key roles in the pentose-phosphate pathway (PPP) (Fig. 4*I*; see also schematic diagram in Fig. 7 and detailed list in *SI Appendix*, Fig. S7). Consistently, we found that NADPH (the product of the PPP pathway) was significantly lower in shARRB1 organoids compared with NTC organoids, leading to an increased NADP/NADPH ratio (Fig. 4*J*).

Elevated glycolysis could lead to increased glucose uptake and accumulation of lactate (26), while elevated OXPHOS is accompanied by increased mitochondrial membrane potential (MMP) and reactive oxygen species (ROS) production. Therefore, we further measured the levels of these four key indicators to confirm the observed metabolic pattern in shARRB1 organoids. As expected, NTC organoids consumed significantly more glucose and secreted more lactate into the medium (Fig. 4*J*). In contrast, shARRB1 organoids showed increased ROS (*SI Appendix*, Fig. S8*A*) and an elevated expression of NRF2 (*SI Appendix*, Fig. S8*B*), a master regulator of cellular ROS. In addition, MMP levels were increased after ARRB1 knockdown (*SI Appendix*, Fig. S8 *C* and *D*), which was consistent with the elevated OXPHOS.

As aforementioned, ARRB1 could interact with E2F1 in the nucleus, and several studies indicated E2F1 regulation of

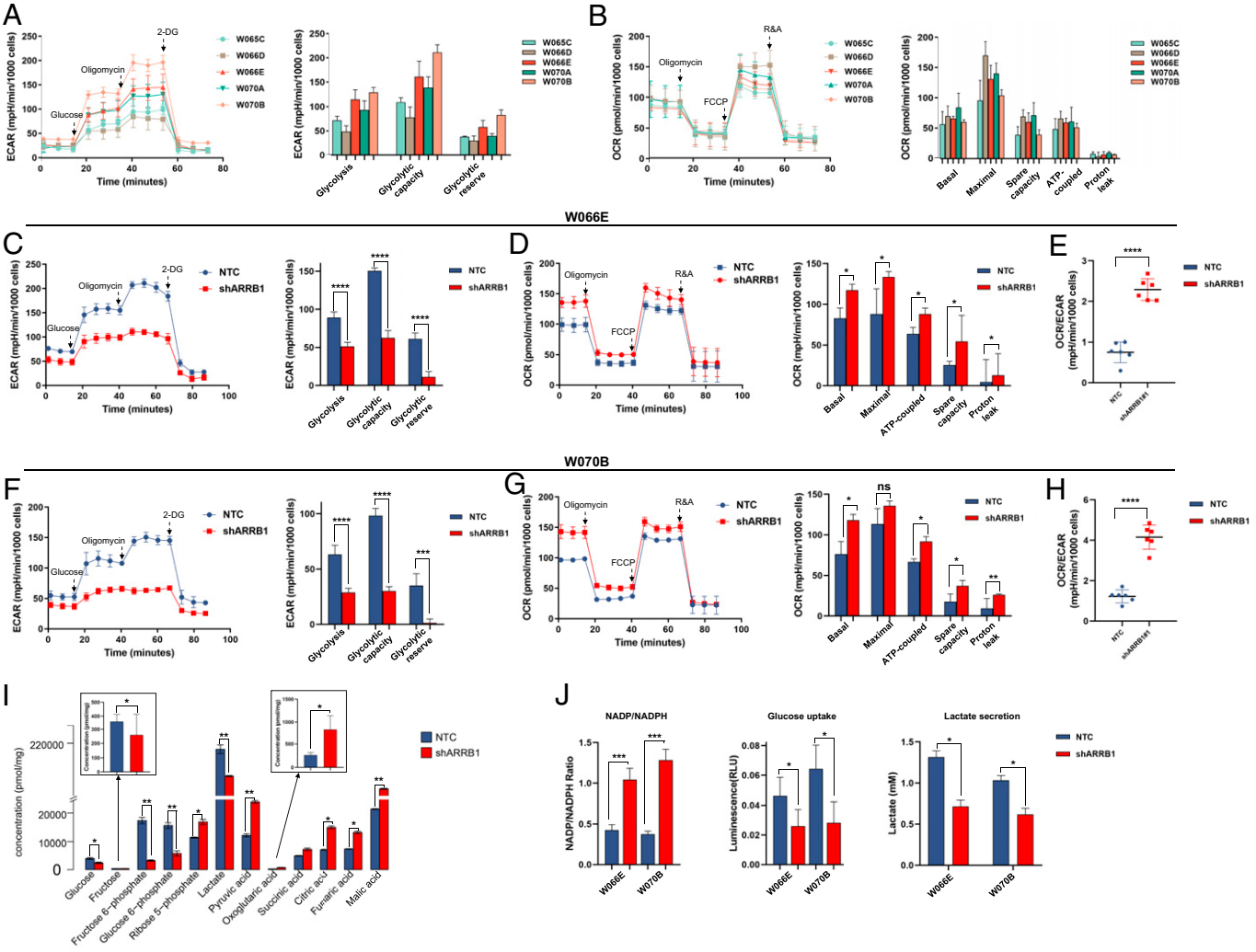

Fig. 4. ARRB1 promotes glycolysis in GC organoids. (*A* and *B*) ECAR and OCR measured for all five organoids using the Seahorse XF-96 analyzer. All the values were normalized to cell numbers. Bar graphs indicate mean and error bars denote SD from six wells (from two experiments). (*A*) Representative traces of ECAR values from a glycolysis stress test, in which glycolysis, glycolytic capacity, and glycolytic reserve were computed. 2-DG, 2-deoxy-D-glucose. (*B*) Representative traces of OCR values from a mitochondrial stress test, in which basal respiration, maximal respiration, spare respiratory capacity, ATP-coupled respiratory capacity, and proton-leak were computed. R&A, rotenone and antimycin A. (*C*) Representative traces of ECAR values from a glycolysis stress test of shARRB1 and NTC organoids (W066E), in which quantification showing decreased glycolysis, glycolytic capacity, and glycolytic reserve in shARRB1 organoids compared with NTC. (*D*) Representative traces of OCR values from a mitochondrial stress test of shARRB1 and NTC organoids (W066E), in which quantification showing increased basal respiration, maximal respiration, ATP-coupled respiratory capacity, spare respiratory capacity, and proton leak in shARRB1 organoids compared with the NTC. (*E*) Plots showing the elevated ratio of OCR to ECAR in shARRB1 organoids compared to the NCT (W066E). *F–H* are counterparts of *C–E* for W070B organoids. (*I*) LC/MS measurements of intracellular concentrations of glycolysis and TCA cycle intermediates in shARRB1 W070B organoids, compared with NTC. (*J*) Bar graphs showing NADP/NADPH ratio, glucose uptake and lactate secretion in two shARRB1 organoids (W066E and W070B), compared with the corresponding NTC. Plots show mean and SD of three technical replicates. *P* value computed using a two-sided Student's *t* test; ****$P < 0.0001$, ***$P < 0.001$, **$P < 0.01$, *$P < 0.05$.

oxidative metabolism in muscle and brown adipose tissues, as well as in colon and lung tissues (27–29). Therefore, we also assessed whether E2F1 is involved in ARRB1-medidated metabolic switch. By measuring ECAR and OCR, we found that E2F1 knockdown has no significant influence on glycolysis in both W066E (*SI Appendix*, Fig. S9 *A*, *Left*) and W07B (*SI Appendix*, Fig. S9 *B*, *Left*) organoids, but significantly increased mitochondrial respiration capacity in both organoid lines, especially with maximal and spare respiration capacities (*SI Appendix*, Fig. S9 *A* and *B*, *Right*). As ARRB1 knockdown led to a significant increase in glycolysis (Fig. 4 *C* and *F*), it is likely that ARRB1 regulation of energy metabolism could be independent of E2F1 regulation in GC. Furthermore, we used the *ARRB1-Q394L* mutant, which has been shown to prevent the translocation of ARRB1 to the nucleus (30), to reveal the subcellar localization dependency of ARRB1-mediated regulation of GC metabolism. Seahorse analysis results showed that overexpression of both wild-type *ARRB1* and *ARRB1-Q394L* mutants significantly rescued the glycolysis compared with the empty vector control in both shARRB1 organoid lines (*SI Appendix*, Fig. S9*C*). Therefore, nuclear translocation of ARRB1 may not be necessary for ARRB1-medidated up-regulation of glycolysis.

Taken together, these results demonstrated that cytoplasmic ARRB1 could induce a metabolic reprogramming from mitochondrial oxidative phosphorylation to glycolysis in GC.

ARRB1 Interacts with PKM2 and Reduces Pyruvate Kinase Activity. We then sought to determine the underlying mechanisms of ARRB1 mediation of metabolic reprogramming. As the first step, we proceeded to identify cellular interacting partners of ARRB1 by coimmunoprecipitation (co-IP) of cell lysates of W070B organoids. After silver staining, bands not shown in the IgG control lane were subjected to MS analysis. The most specific

band in the anti-ARRB1 lane led to identification of 10 high-confidence interacting proteins with confirmation of a duplicate co-IP/MS analysis (Dataset S3), in which PKM2 showed the highest protein abundances with support of multiple identified peptides (Fig. 5*A*). The interaction with PKM2 was also identified in a global proteomic analysis of ARRB1 interactome in HEK293 cells with stable overexpression of a FLAG-tagged version of ARRB1, but its biological function remained unknown (31). PKM2 is a pivotal enzyme of tumor metabolism regulation, which catalyzes the last step of glycolysis by transferring the phosphate from phosphoenolpyruvate to ADP to yield ATP and pyruvate (32). Endogenous ARRB1–PKM2 interaction was confirmed by reciprocal co-IP in both W070B and W066E organoids (Fig. 5*B*). Moreover, the binding ability of recombinant GST-ARRB1 and His-PKM2 proteins was measured using binding ELISAs for further validation. As shown in Fig. 5*C*, ARRB1 can bind PKM2 with a linear range of 0.00625 to 2 μg/mL, and vice versa. In addition, we investigated the ARRB1–PKM2 interaction in human GC samples by proximity ligation assay (PLA) (Fig. 5*D* and *SI Appendix*, Fig. S10*A*). PLA is a method to identify physical closeness of proteins, where a fluorescence signal will only be produced if two proteins of interest are in close proximity with less than 40 nm in tissue sections. Positive fluorescence signals were detected in all tested samples, compared to negative control (*SI Appendix*, Fig. S10*A*). Fluorescence intensities in GC tumors with higher ARRB1 protein levels (e.g., G0302, G0177, G0369) were found to be more intense than those with lower ARRB1 protein levels (e.g., G0190, G0104, G0315) (*SI Appendix*, Fig. S10*A*). Notably, positive signals mostly located in the cytoplasm, but in a sample with only nuclear ARRB1 localization (G0142), interaction signals were localized in the nucleus as well (*SI Appendix*, Fig. S10). Together, multiple orthogonal assays demonstrated an endogenous interaction of ARRB1 with PKM2.

Subsequently, we investigated the effect of ARRB1 interaction with PKM2. Knockdown of ARRB1 had no influence on PKM2 protein abundances (Fig. 5 *E*, *Left*), but led to sixfold increase of pyruvate kinase activity in W070B organoids and twofold increase in W066E organoids (Fig. 5 *E*, *Right*), indicating that ARRB1 interaction with PKM2 may significantly reduce pyruvate kinase activity. The higher level of pyruvate kinase activity increase after ARRB1 knockdown in W070B organoids than W066E organoids may be associated with the higher basal expression of ARRB1 in W070B organoids (Fig. 2 *A*–*C*). As low PKM2 activity has been associated with elevated lactate production in cancer (33, 34), we speculated that inhibition of PKM2 may be the mechanism underlying ARRB1 mediation of metabolic reprogramming, and further tested whether reduced glycolysis by ARRB1 knockdown could be rescued by reinhibition of PKM2. ECAR was measured in shARRB1 organoids after exposure to a PKM2 specific inhibitor (compound 3k), and the results demonstrated that reinhibition of PKM2 significantly restores glycolysis capacity in ARRB1 knockdown organoids (Fig. 5*F*).

Our next question was how ARRB1 binding reduces PKM2 activity. PKM2 activity has been known to be associated with its multimeric forms: a nearly inactive monomer/dimer and an enzymatically active tetramer (33). As switching between different forms is the key of PKM2 activity regulation, we evaluated whether ARRB1 interferes with the monomer–dimer–tetramer equilibrium of PKM2. We performed size-exclusion chromatography to determine the stoichiometry of the full composition of PKM2 subunits. Immunoblotting of each fraction revealed that shARRB1 organoids depicted higher proportions of tetramer forms and lower proportions of monomer forms than NTC organoids, in both W066E and W070B organoid lines (Fig. 5*G*), suggesting that ARRB1 could disrupt the stabilization of PKM2 tetramers and promote the monomeric form. Together, these results indicated that ARRB1 interaction with PKM2 may reduce its kinase activity through interfering with the monomer–dimer–tetramer equilibrium of PKM2, which could promote glucose flux into glycolysis (Fig. 5*H*).

We further sought to determine the minimal region crucial for the ARRB1–PKM2 interaction. N terminal- and C terminal-truncated mutants fused to Flag-tag for ARRB1 were generated, respectively. W070B organoids were transfected with these Flag-ARRB1 mutants, followed by IP and Western blotting analysis. The N domain (Δ1) and C domain (Δ2) of ARRB1 were both involved in ARRB1–PKM2 interaction, as shown in Fig. 5*I*. Moreover, as reported, mammalian ARRB1 existed in a constitutively phosphorylated state in the cytosol (3), and PKM2 can interact with proteins harboring phosphorylated tyrosine residues, leading to its activity reduction (35). Therefore, another two ARRB1 mutants, with known tyrosine phosphorylation sites (Y47/54/63/144/173, based on information from PhosphositePlus) mutated (Δ3) or all known phosphorylation sites (tyrosine, serine, or threonine phosphorylation) mutated (Δ4), were generated. Surprisingly, both mutant forms of phosphorylation sites did not disrupt the interaction between ARRB1 and PKM2 (Fig. 5*I*), indicating ARRB1 phosphorylation status may be not essential for ARRB1–PKM2 interaction. We also performed the reciprocal experiment for PKM2 and generated truncated mutants fused to Flag-tag for PKM2, and found PKM2 domain N/A1 (Δ1), B (Δ2), and C (Δ6) may be involved in the interaction, as the mutant deleting these domains (Δ5) abolished the interaction (Fig. 5*J*). These results indicated that there might be multiple binding sites between ARRB1 and PKM2.

The localization of these ARRB1 mutants were further analyzed by subcellular fractionation analysis of W066E and W070B organoids with overexpression of respective ARRB1 mutants (*SI Appendix*, Fig. S11 *A* and *B*). We found that FL, Δ3, and Δ4 mutants were predominantly localized in the cytoplasm. The Δ1 mutant showed an evident nuclear accumulation, which was previously reported indispensable for the nuclear localization of β-arrestins (36); while Δ2 was distributed throughout the nucleus and cytoplasm, possibly because its C domain (residues 188 to 362) does not include the functional NES (residues 385 to 396) located at the C terminus of ARRB1. The Δ5 (ARRB1-Q394L) mutant showed a clear exclusion from the nucleus as expected. The same pattern was observed in both organoid lines (*SI Appendix*, Fig. S11 *A* and *B*).

We further assessed the effects of different ARRB1 mutants on PKM2 activity. Overexpression of the Δ5 (ARRB1-Q394L) mutant showed the greatest degree of PKM2 activity inhibition, followed by FL, Δ2, Δ4, Δ3, and Δ1 mutants (Fig. 5 *K*, *Left*). This result demonstrated that exclusion of ARRB1 from nucleus enhances the inhibitory effect on PKM2 activity, and the interference of PKM2 activity by ARRB1 may be modulated via the C domain (as the Δ1 mutant with the N domain exerting the least effect) and might be related with phosphorylation status as well. Further size-exclusion chromatography and subsequent fraction analysis presented a consistent result, in which overexpression of the Δ5 mutant resulted in a shift of PKM2 into a monomeric configuration compared with full length (FL), whereas overexpression of other mutants led to a more tetrameric configuration (Fig. 5 *K*, *Right*; uncropped images showed in *SI Appendix*, Fig. S11*C*).

Finally, as PKM2 could also translocate into the nucleus upon EGF induction (37), we evaluated whether the subcellular localization change of ARRB1 was coupled with PKM2.

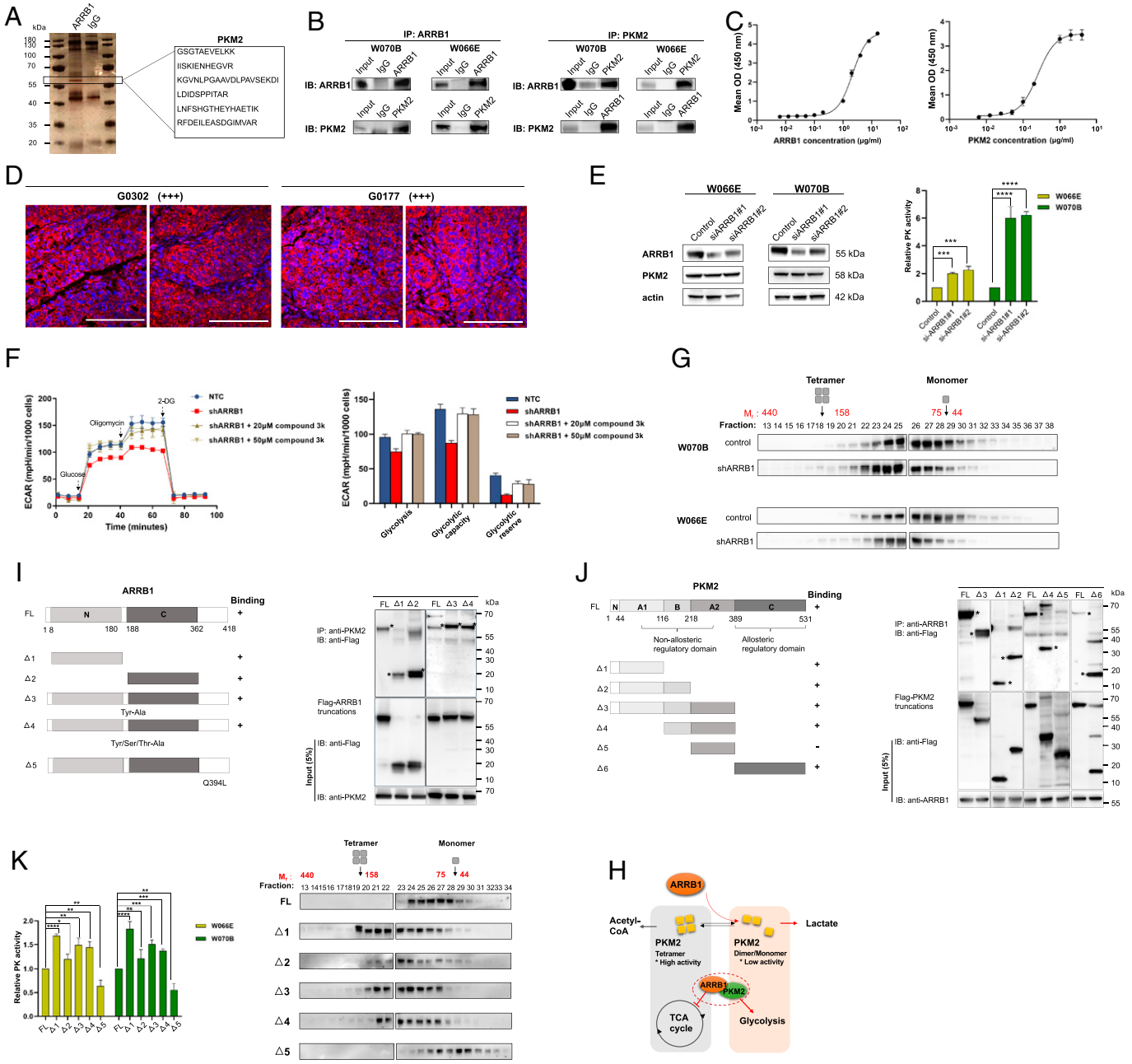

Fig. 5. ARRB1 interacts with PKM2. (*A*) Co-IP followed by MS analysis identified ARRB1 association with PKM2. Silver-stained gel showing the proteins that bind to ARRB1 in comparison with IgG (*Left*), with annotation of the peptides from PKM2 that were identified by MS analysis (*Right*). (*B*) IP assays performed with IgG, anti-ARRB1 and anti-PKM2 antibodies in W070B and W066E organoids, followed by Western blotting analysis. (*C*) Linear curves from reciprocal ELISA binding assay analyses, demonstrating the binding between ARRB1 and PKM2. (*D*) Representative images of PLA for human GC samples. (Scale bars, 100 μm.) (*E*) Western blots of PKM2 for two siARRB1 organoids in comparison with control (*Left*), and bar graphs (*Right*) showing pyruvate kinase (PK) activity change after ARRB1 knockdown. Data shown as mean ± SD of three technical replicates. *P* value computed using a two-sided Student's *t* test; ****$P < 0.0001$, ***$P < 0.001$. (*F*) PKM2 activity inhibition rescued the decreased glycolysis caused by ARRB1 knockdown. ECAR was measured for shARRB1 organoids treated with the indicated doses of a PKM2 inhibitor (compound 3k) for 3 h, as well as NTC and untreated shARRB1 organoids. Representative traces of ECAR values are shown (*Left*); glycolysis, glycolytic capacity and glycolytic reserve in ECAR were computed and shown (*Right*). Data shown as mean ± SD from six wells (from two experiments). (*G*) The stoichiometry of PKM2 subunit association determined by Western blotting of the chromatographic fractions of shARRB1 organoids and NTCs (W070B and W066E). Organoid lysates were separated and analyzed by size-exclusion chromatography. M_r, relative molecular weight. Uncropped blots shown in *SI Appendix*, Fig. S12*A*. Proteins of two groups were loaded with equal amounts (5 mg). (*H*) The proposed model depicting ARRB1 as a major regulator in PKM2-stimulated metabolic reprogramming. (*I* and *J*) Determination of minimal ARRB1–PKM2 interaction region. Co-IP analyses were performed with an anti-PKM2 (*I*) or anti-ARRB1 (*J*) antibody in W070B organoids, transfected with Flag-ARRB1 plus one of a series of N-terminal or C-terminal ARRB1 truncates (*I*); or Flag-PKM2 plus one of a series of N-terminal or C-terminal PKM2 truncates (*J*). Interaction-competent truncates are indicated by asterisks (*) in each schematic. (*K*, *Left*) Bar graphs showing pyruvate kinase activity change after transfection with Flag-ARRB1 plus one of a series of N-terminal or C-terminal ARRB1 truncates, in W066E and W070B organoids. (*Right*) The stoichiometry of PKM2 subunit association determined by Western blots of the chromatographic fractions of W070B organoids transfected with Flag-ARRB1 plus individual ARRB1 truncate. *P* value computed using a two-sided Student's t-test; ****$P < 0.0001$, ***$P < 0.001$, **$P < 0.01$, *$P < 0.05$. Uncropped blots are shown in *SI Appendix*, Fig. S11*C*.

Immunofluorescent staining was performed in W070 organoids at day 1 and day 7 after passage. We found that a large amount of ARRB1 translocated into the nucleus at day 1, while only a small amount of nuclear PKM2 were observed (*SI Appendix*, Fig. S11*D*). Therefore, the nuclear translocation of ARRB1 may be independent of PKM2, but their colocalization in the cytoplasm at day 7 confirmed the interaction and functional association of these two proteins described above.

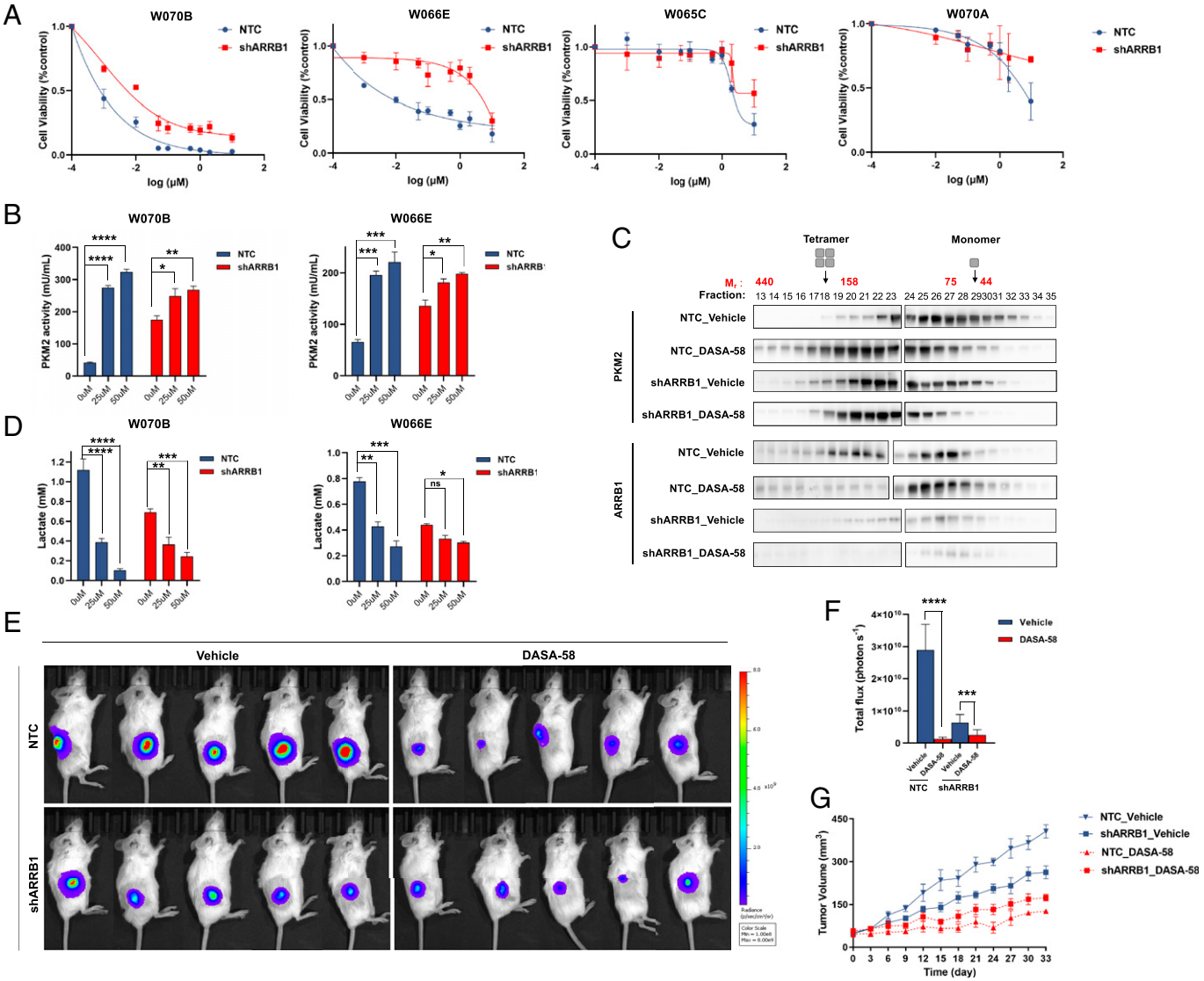

Fig. 6. PKM2 activation as a potential therapeutic strategy in GC with high ARRB1 expression. (*A*) Dose–response curves of ARRB1 high (W070B and W066E) and ARRB1 low (W065C and W070A) GC organoids treated with PKM2 activator DASA-58 with indicated concentrations ($n = 3$). (*B*) PKM2 activity of control and shARRB1 organoids (W070B and W066E), treated with indicated concentrations of DASA-58 for 3h ($n = 3$). Data shown as mean ± SD *P* value computed using a two-sided Student's *t* test; ****$P < 0.0001$, ***$P < 0.001$, **$P < 0.01$, *$P < 0.05$. (*C*) The stoichiometry of PKM2 and ARRB1 subunit association determined by Western blots of the chromatographic fractions of NTC and shARRB1 organoids (W070B), with treatment of DASA-58 (50 μM) for 3 h or vehicle (uncropped blots shown in *SI Appendix*, Fig. S12 *B* and *C*). (*D*) Lactate secretion of control and shARRB1 organoids (W070B and W066E) treated with indicated concentrations of DASA-58 for 3h ($n = 3$). (*E*) Luciferase-labeled W070B-NTC and W070B-shARRB1 organoids were subcutaneously implanted into nod/scid mice and subjected to DASA-58 and vehicle treatment ($n = 5$). Tumor burden was calculated by luciferase intensity quantifications (detailed values shown in *SI Appendix*, Fig. S13*C*) at day 33. (*F*) Bar graphs comparing tumor burden (represented by total photon flux) between vehicle and DASA-58 treatment groups in NTC and shARRB1 organoids derived xenografts, respectively. Statistical significances of differences between treatment and corresponding vehicle groups were assessed by ANOVA and post hoc Tukey HSD test. (*G*) Longitudinal tumor volume curves for each group of xenografts. ****$P < 0.0001$, ***$P < 0.001$, **$P < 0.01$, *$P < 0.05$.

ARRB1^{high} Organoids Were More Sensitive to PKM2 Activation Treatment. Inducing biased responses through β-arrestins has become an active research area. Several biased agonists have begun to advance in clinical development, while therapeutic antagonists are still at an early stage (38). Therefore, considering that PKM2 is mostly expressed in proliferating cells, especially in tumors studied thus far (39), we explored the therapeutic potential of activating PKM2 in GC, as inhibiting PKM2 activity by ARRB1 interaction could promote aerobic glycolysis and tumor proliferation. Selective PKM2 activators TEPP-46 and DASA-58, which could promote the stable association of PKM2 subunits (40), were evaluated in four organoid lines. DASA-58 treatment showed higher antiproliferation efficacy than TEPP-46 (*SI Appendix*, Fig. S13*A*), and ARRB1^{high} organoids (W070B and W066E) tended to be more sensitive to DASA-58 treatment compared with ARRB1^{low} organoids (W065C and W070A) (Fig. 6*A*). We also observed that DASA-58 treatment inhibited the proliferation of NTC organoids more effectively compared with ARRB1 knockdown organoids, which was especially obvious in ARRB1^{high} organoid lines (Fig. 6*A*). Consistently, DASA-58 significantly elevated the PKM2 activity in NTC organoids compared with shARRB1 organoids (Fig. 6*B*).

We further confirmed this finding by size-exclusion chromatography analysis of an ARRB1^{high} organoid line (W070B). As shown in Fig. 6*C*, exposure of NTC organoids to DASA-58 resulted in a shift of PKM2 protein into a more tetrameric configuration, whereas treated shARRB1 organoids only depicted a partial shift of PKM2 into tetramers, which was consistent with the sensitivity difference observed between NTC and shARRB1 organoids to DASA-58 (Fig. 6*B*). This may be due to a high basal

PKM2 activity in shARRB1 organoids, limiting the extent of additional increase of PKM2 activity (represented by the proportion of tetramer forms) in response to DASA58 treatment. At the same time, we observed that ARRB1 depicted an opposite shift after DASA-58 treatment, indicating at least partial disruption of ARRB1–PKM2 complex by DASA-58 (Fig. 6*C*). Moreover, size-exclusion chromatography was also applied to another ARRB1^{low} organoid line (W070A). The basal proportions of PKM2 tetramer forms in W070A (*SI Appendix*, Fig. S13*B*; uncropped images shown in *SI Appendix*, Fig. S13*D*) was found to be higher than W070B (Fig. 6*C*) as expected. Due to its high basal tetramer proportions, both NTC and shARRB1 groups depicted a limited shift of PKM2 protein to a more tetrameric configuration after treatment with DASA-58 (not as obvious as W070B), which may account for its less sensitivity to DASA-58.

To investigate whether DASA-58 could reverse ARRB1 induced metabolic state, lactate levels were measured in ARRB1^{high} organoids (W070B and W066E) after exposure to DASA-58. We observed that DASA-58 treatment significantly reduced the lactate levels in NTC organoids compared with shARRB1 organoids in both organoid lines (Fig. 6*D*). Furthermore, we validated the impact of ARRB1 inhibition in vivo, xenograft treatment assays (using W070B organoids-derived xenograft) were conducted and analyzed. Consistently, we observed decreased tumor growth in DASA-58–treated mice compared with vehicle-treated controls in both NTC and shARRB1 groups (Fig. 6 *E*–*G*). Notably, NTC organoids-derived tumors depicted higher sensitivity than shARRB1 tumors (Fig. 6 *F* and *G*), implying tumors with high levels of ARRB1 may benefit more from DASA-58 treatment. Taken together, PKM2 activator DASA-58 could attenuate the proliferation-promoting function by ARRB1–PKM2 axis, especially in ARRB1^{high} tumors.

Discussion

ARRB1 regulates a wide array of important cellular functions with physiological and pathophysiological relevance (1). Recent analyses of mice lacking or overexpressing ARRB1 indicated a role of ARRB1 in maintaining glucose homeostasis in adipocytes, pancreatic β-cells, and Agouti-related protein (AgRP)-expressing neurons (41). Metabolic alteration is an essential hallmark of cancer, and a better understanding of the mechanistic links between cellular metabolism and growth control could lead to development of better cancer treatments. In this study, we identify a role of ARRB1 in Warburg effect regulation through its interaction with PKM2, which hinders PKM2 tetramerization and reduces its pyruvate kinase activity.

Pyruvate kinase is located at a "gate" position in the glycolytic flux to respond to various stimuli (33), which activities determine the subsequent metabolic flow to anabolic or catabolic processes. Specific pyruvate kinase isoforms (PKM1 and PKM2) of the *PKM* gene have been indicated to support divergent energetic and biosynthetic requirements of cells in tumors and normal tissues, due to different kinetic and regulatory properties. PKM1 is found predominantly in differentiated adult tissues with high ATP requirements, whereas PKM2 is mostly expressed in proliferating cells, including in cancer cell lines and tumors studied thus far (39). This expression pattern holds in GC samples based on our RNA-seq profiles. Moreover, different from PKM1 that forms a stable and constitutively active tetramer, PKM2 normally presents a dimeric form with low catalytic activity in cancer cells (39), which is associated with elevated aerobic glycolysis to accumulate glycolytic intermediates for biosynthetic reaction to support cancer cell proliferation. Although replacement of PKM2 with PKM1 in cultured cells limits flux through anabolic pathways, thereby preventing xenograft tumor formation (42), recent studies demonstrated that PKM2 knockout mice models strikingly accelerated tumor formation in specific context, possibly due to a low level of compensatory PKM1 expression (43, 44), indicating the metabolic regulatory network involving PKM2 is more elaborate than previously thought in cancer. Together, it underscores the importance to elucidate PKM isoform expression and the mechanism to modulate the enzymatic activity in GC.

It has been known that the enzymatic activity of PKM2 could be allosterically triggered endogenously by fructose-1,6-bisphosphate (FBP), serine, and SAICAR (an intermediate of the de novo purine nucleotide synthesis pathway), as well as exogenously by synthetic compounds DASA-58 and TEPP-46 (40). In contrast, phosphotyrosine-containing proteins could negatively affect the pyruvate kinase activity of PKM2 (34, 45). Our data suggest that ARRB1 interaction with PKM2 represents a metabolic switch favoring the biosynthetic route, including the pentose phosphate pathway as indicated by the rewired metabolomic profiles in GC organoids (Fig. 7). We also demonstrated that ARRB1^{high} GC preclinical models were sensitive to PKM2 activator DASA-58. Unlike FBP, DASA-58 binding to PKM2 promotes a constitutively active enzyme state, which is resistant to inhibition by tyrosine-phosphorylated proteins (40).

Another interesting finding of this study is that subcellular localization of ARRB1 is time-dependent during a passage of GC organoid cultures. ARRB1 mostly located in the cytoplasm in investigated GC patient samples, which may be due to the high density of cells in human tumor tissue. Therefore, we investigated whether the subcellular localization of ARRB1 differs between fast-growing tumor margins and interior. IHC staining of seven regions of a human GC surgical tumor (diameter > 2 cm) showed that ARRB1 was mostly localized in the cytoplasm in tumor interior (*SI Appendix*, Fig. S14*A*), whereas nuclear localization of ARRB1 was observed in a substantial portion of cells at tumor margins in some regions (three of seven), especially in gastric muscular proprietary invasion lesions (*SI Appendix*, Fig. S14*A*). This subcellular localization difference was not observed in tumors of organoid-derived xenografts (diameter: 0.5 to 1 cm), possibly because investigated xenograft tumors were small and without gastric anatomical structure. Moreover, we observed strong nuclear ARRB1 staining in dividing cells (*SI Appendix*, Fig. S14*B*) and in small organoids, while big organoids depicted cytoplasmic localization (*SI Appendix*, Fig. S14*C*), further supporting an association of nuclear ARRB1 with GC cell proliferation states.

Regarding the mechanism underlying the cytonuclear trafficking, we showed that ARRB1 translocation into the nucleus is dependent on EGF. Therefore, we tested whether Src is involved in the nuclear translocation of ARRB1, as Src could be bound with ARRB1 to transactivate EGF receptors (1, 46). We found that Src was activated upon EGF addition, marked by its increased p-Src (Y416) levels (*SI Appendix*, Fig. S15*A*), but double-immunofluorescence results of ARRB1 with p-Src or Src showed that only ARRB1 translocated into the nucleus at day 1 to 2 after passage, while Src (*SI Appendix*, Fig. S15*B*) and p-Src (*SI Appendix*, Fig. S15*C*) showed the cytoplasmic and membrane localization. Additionally, it has been suspected that coexpression with ARRB2 (formation of hetero-oligomerization) may cause cytosolic retention of ARRB1, as ARRB2 is constitutively exported from the nucleus due to its NES sequence (3, 21). Therefore, we tested this idea using the RNA-seq profiles, and found significant up-regulation of ARRB2 at day 3 (*SI Appendix*, Fig. S16*A*), associated with the observed subcellular localization transition of ARRB1 at this time point. Furthermore, we compared protein

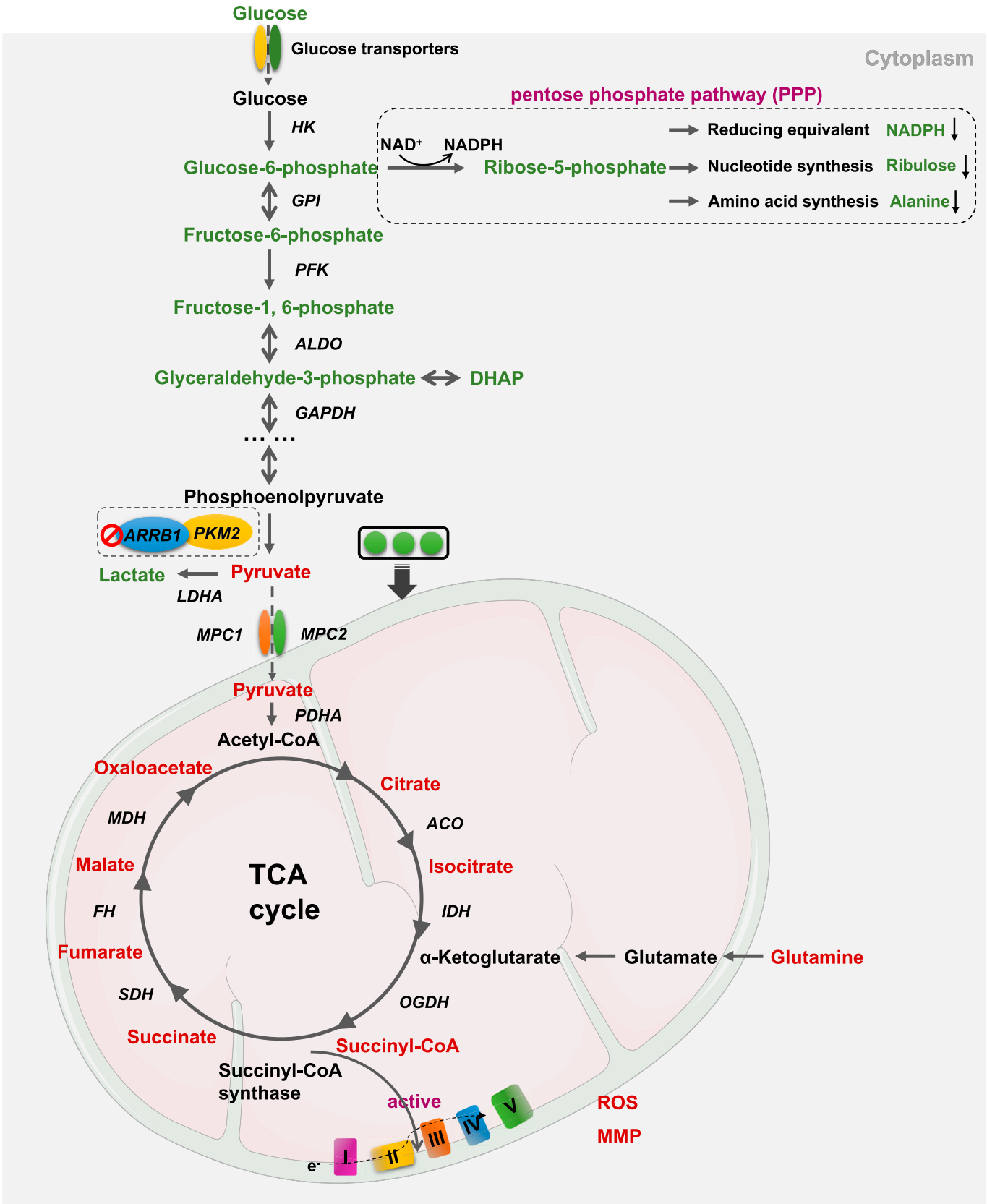

Fig. 7. ARRB1-mediated effect on GC cellular metabolism. Schematic diagram illustrating altered metabolites of glycolytic pathway and TCA cycle that are mediated by ARRB1. Metabolites showing increased concentration in shARRB1 organoids are labeled in red, while decreased ones in green.

abundances of ARRB1 and ARRB2 using published datasets. The ARRB1/ARRB2 ratio was significantly lower in GC than in prostate cancer (*SI Appendix*, Fig. S16*B*), agreeing with subcellular distribution of ARRB1 in these two cancer types, in which ARRB1 mostly localized in the cytoplasm in GC and 50% cases had strong nuclear ARRB1 intensity in prostate cancer (11). This

difference of subcellular distribution may also explain another ARRB1-mediated metabolic route observed in prostate cancer, which was via inducing pseudohypoxia through regulation of HIF1A transcriptional activity in the nucleus, to down-regulate SDHA and FH expression (11). These analyses indicate that the subcellular localization of ARRB1 needs to be taken into consideration when assessing ARRB1 expression and elucidating its function, although further investigation is needed to reveal the exact mechanism.

Together, the data in our study warrant future research into the intricate ARRB1-mediated signaling pathways in GC, which may facilitate the development of therapeutic strategies to target metabolic vulnerability in cancer cells.

Materials and Methods

Establishment and Passage of Organoid Cultures. GC organoids establishment referenced the previously published protocol (47) with modifications (48). Tumor samples underwent three to five washes with PBS (1% penicillin-streptomycin and 5% amphotericin B). Tissues were minced into small pieces about 1 to 5 mm^2 and then digested in 5 to 10 mL of 5 mg/mL collagenase type I (Invitrogen) in Advanced DMEM/F12 (Invitrogen) containing 10 μM Y27632, 2.5%FBS and 1%P/S for 1 to 2 h at 37 °C gently shaking. Then, cell cluster-containing supernatant was collected and centrifuged at 600 × *g* for 5 min. Cell pallet was washed three times using Advanced DMEM/F12 and resuspended in growth factor reduced Matrigel (BD Biosciences). A drop of 50 μL Matrigel–cell mixture was added to each well of a prewarmed 24-well plate. After the drops solidified by a 30-min 37 °C incubation, 500 μL of gastric organoid medium was added to each well. Fresh medium was changed every 2 to 3 d. Organoids formed after 1 to 3 d. Passage of the organoid cultures was performed 7 to 10 d after isolation. GC organoids were passaged by incubating in TryplE (Invitrogen) at 37 °C for 5 min.

Tissue, Molecular, Animal, and Statistical Analyses. For details regarding tumor samples, siRNA and plasmid transfection, lentivirus transduction, qRT-PCR, RNA-seq, IHC, Western blotting, co-IP assay, functional ELISAs, tissue respirometry, ECAR and OCR assays, measurement of lactate, ROS, NAD/NADPH ratio and MMP, metabolic profiling, measurement of PK activity and glucose uptake ability, size-exclusion chromatography, cell viability assay, animal studies, and statistical analyses, refer to *SI Appendix*.

Data, Materials, and Software Availability. The RNA-seq data reported in this study have been deposited in the GSA for Human repository, https://ngdc.cncb.ac.cn/gsa-human/ (accession no. HRA002205) (49).

ACKNOWLEDGMENTS. We thank the patient and their families who participated in this study; and Ying Liu from Peking University and Daming Gao from State Key Laboratory of Cell Biology, Chinese Academy of Sciences for suggestions on experiment design. This study was supported by Beijing Municipal Science and Technology Commission (Z201100008320006); Peking University-Baidu Fund (2019BD012); National Natural Science Foundation of China (82273253); and the third round of Public Welfare Development and Reform Pilot Projects of Beijing Municipal Medical Research Institutes (Beijing Medical Research Institute, 2019-1).

1. S. Ahn, S. K. Shenoy, L. M. Luttrell, R. J. Lefkowitz, SnapShot: β-Arrestin functions. *Cell* **182**, 1362–1362.e1 (2020).
2. R. J. Lefkowitz, S. K. Shenoy, Transduction of receptor signals by beta-arrestins. *Science* **308**, 512–517 (2005).
3. S. M. DeWire, S. Ahn, R. J. Lefkowitz, S. K. Shenoy, Beta-arrestins and cell signaling. *Annu. Rev. Physiol.* **69**, 483–510 (2007).
4. A. K. Shukla, K. Xiao, R. J. Lefkowitz, Emerging paradigms of β-arrestin-dependent seven transmembrane receptor signaling. *Trends Biochem. Sci.* **36**, 457–469 (2011).
5. L. M. Luttrell *et al.*, Activation and targeting of extracellular signal-regulated kinases by beta-arrestin scaffolds. *Proc. Natl. Acad. Sci. U.S.A.* **98**, 2449–2454 (2001).
6. D. S. Witherow, T. R. Garrison, W. E. Miller, R. J. Lefkowitz, Beta-arrestin inhibits NF-kappaB activity by means of its interaction with the NF-kappaB inhibitor IkappaBalpha. *Proc. Natl. Acad. Sci. U.S.A.* **101**, 8603–8607 (2004).
7. J. Kang *et al.*, A nuclear function of beta-arrestin1 in GPCR signaling: Regulation of histone acetylation and gene transcription. *Cell* **123**, 833–847 (2005).
8. Y. Yang *et al.*, β-Arrestin1 enhances hepatocellular carcinogenesis through inflammation-mediated Akt signalling. *Nat. Commun.* **6**, 7369 (2015).
9. F. G. Buchanan *et al.*, Role of beta-arrestin 1 in the metastatic progression of colorectal cancer. *Proc. Natl. Acad. Sci. U.S.A.* **103**, 1492–1497 (2006).
10. S. K. Shenoy *et al.*, β-Arrestin1 mediates metastatic growth of breast cancer cells by facilitating HIF-1-dependent VEGF expression. *Oncogene* **31**, 282–292 (2012).
11. V. Zecchini *et al.*, Nuclear ARRB1 induces pseudohypoxia and cellular metabolism reprogramming in prostate cancer. *EMBO J.* **33**, 1365–1382 (2014).
12. P. Dasgupta *et al.*, ARRB1-mediated regulation of E2F target genes in nicotine-induced growth of lung tumors. *J. Natl. Cancer Inst.* **103**, 317–333 (2011).
13. S. Pillai *et al.*, β-arrestin-1 mediates nicotine-induced metastasis through E2F1 target genes that modulate epithelial-mesenchymal transition. *Cancer Res.* **75**, 1009–1020 (2015).
14. Y. Shu *et al.*, ARRB1-promoted NOTCH1 degradation is suppressed by OncomiR miR-223 in T-cell acute lymphoblastic leukemia. *Cancer Res.* **80**, 988–998 (2020).
15. D. Son *et al.*, miR-374a-5p promotes tumor progression by targeting ARRB1 in triple negative breast cancer. *Cancer Lett.* **454**, 224–233 (2019).
16. H. Sung *et al.*, Global cancer statistics 2020: GLOBOCAN estimates of incidence and mortality worldwide for 36 cancers in 185 countries. *CA Cancer J. Clin.* **71**, 209–249 (2021).
17. L. Yang *et al.*, Gastric cancer: Epidemiology, risk factors and prevention strategies. *Chin. J. Cancer Res.* **32**, 695–704 (2020).
18. N. N. Pavlova, C. B. Thompson, The emerging hallmarks of cancer metabolism. *Cell Metab.* **23**, 27–47 (2016).
19. G. Kroemer, J. Pouyssegur, Tumor cell metabolism: Cancer's Achilles' heel. *Cancer Cell* **13**, 472–482 (2008).
20. S. Ge *et al.*, A proteomic landscape of diffuse-type gastric cancer. *Nat. Commun.* **9**, 1012 (2018).
21. L. Ma, G. Pei, Beta-arrestin signaling and regulation of transcription. *J. Cell Sci.* **120**, 213–218 (2007).
22. H. C. H. Lau, O. Kranenburg, H. Xiao, J. Yu, Organoid models of gastrointestinal cancers in basic and translational research. *Nat. Rev. Gastroenterol. Hepatol.* **17**, 203–222 (2020).
23. D. G. Mun *et al.*, Proteogenomic characterization of human early-onset gastric cancer. *Cancer Cell* **35**, 111–124.e10 (2019).
24. W. El-Rifai, M. Sarlomo-Rikala, L. C. Andersson, S. Knuutila, M. Miettinen, DNA sequence copy number changes in gastrointestinal stromal tumors: Tumor progression and prognostic significance. *Cancer Res.* **60**, 3899–3903 (2000).
25. R. Pike, E. Ortiz-Zapater, B. Lumicisi, G. Santis, M. Parsons, KIF22 coordinates CAR and EGFR dynamics to promote cancer cell proliferation. *Sci. Signal.* **11**, eaaq1060 (2018).
26. M. G. Vander Heiden, L. C. Cantley, C. B. Thompson, Understanding the Warburg effect: The metabolic requirements of cell proliferation. *Science* **324**, 1029–1033 (2009).
27. E. Blanchet *et al.*, E2F transcription factor-1 regulates oxidative metabolism. *Nat. Cell Biol.* **13**, 1146–1152 (2011).
28. B. N. Nicolay *et al.*, Proteomic analysis of pRb loss highlights a signature of decreased mitochondrial oxidative phosphorylation. *Genes Dev.* **29**, 1875–1889 (2015).
29. B. N. Nicolay, N. J. Dyson, The multiple connections between pRB and cell metabolism. *Curr. Opin. Cell Biol.* **25**, 735–740 (2013).
30. M. R. Hara *et al.*, A stress response pathway regulates DNA damage through β2-adrenoreceptors and β-arrestin-1. *Nature* **477**, 349–353 (2011).
31. K. Xiao *et al.*, Functional specialization of beta-arrestin interactions revealed by proteomic analysis. *Proc. Natl. Acad. Sci. U.S.A.* **104**, 12011–12016 (2007).
32. F. Liu *et al.*, PKM2 methylation by CARM1 activates aerobic glycolysis to promote tumorigenesis. *Nat. Cell Biol.* **19**, 1358–1370 (2017).
33. W. Luo, G. L. Semenza, Emerging roles of PKM2 in cell metabolism and cancer progression. *Trends Endocrinol. Metab.* **23**, 560–566 (2012).
34. H. J. Wang *et al.*, JMJD5 regulates PKM2 nuclear translocation and reprograms HIF-1α-mediated glucose metabolism. *Proc. Natl. Acad. Sci. U.S.A.* **111**, 279–284 (2014).
35. H. R. Christofk, M. G. Vander Heiden, N. Wu, J. M. Asara, L. C. Cantley, Pyruvate kinase M2 is a phosphotyrosine-binding protein. *Nature* **452**, 181–186 (2008).
36. P. Wang, Y. Wu, X. Ge, L. Ma, G. Pei, Subcellular localization of beta-arrestins is determined by their intact N domain and the nuclear export signal at the C terminus. *J. Biol. Chem.* **278**, 11648–11653 (2003).
37. W. Yang *et al.*, Nuclear PKM2 regulates β-catenin transactivation upon EGFR activation. *Nature* **480**, 118–122 (2011).
38. J. S. Smith, R. J. Lefkowitz, S. Rajagopal, Biased signalling: From simple switches to allosteric microprocessors. *Nat. Rev. Drug Discov.* **17**, 243–260 (2018).
39. T. L. Dayton, T. Jacks, M. G. Vander Heiden, PKM2, cancer metabolism, and the road ahead. *EMBO Rep.* **17**, 1721–1730 (2016).
40. D. Anastasiou *et al.*, Pyruvate kinase M2 activators promote tetramer formation and suppress tumorigenesis. *Nat. Chem. Biol.* **8**, 839–847 (2012).
41. S. P. Pydi *et al.*, Beta-arrestins as important regulators of glucose and energy homeostasis. *Annu. Rev. Physiol.* **84**, 17–40 (2022).
42. H. R. Christofk *et al.*, The M2 splice isoform of pyruvate kinase is important for cancer metabolism and tumour growth. *Nature* **452**, 230–233 (2008).
43. W. J. Israelsen *et al.*, PKM2 isoform-specific deletion reveals a differential requirement for pyruvate kinase in tumor cells. *Cell* **155**, 397–409 (2013).
44. T. L. Dayton *et al.*, Germline loss of PKM2 promotes metabolic distress and hepatocellular carcinoma. *Genes Dev.* **30**, 1020–1033 (2016).
45. L. Lv *et al.*, Mitogenic and oncogenic stimulation of K433 acetylation promotes PKM2 protein kinase activity and nuclear localization. *Mol. Cell* **52**, 340–352 (2013).
46. R. B. Irby, T. J. Yeatman, Role of Src expression and activation in human cancer. *Oncogene* **19**, 5636–5642 (2000).
47. S. Bartfeld *et al.*, In vitro expansion of human gastric epithelial stem cells and their responses to bacterial infection. *Gastroenterology* **148**, 126–136.e6 (2015).
48. M. Wang *et al.*, In-depth comparison of matrigel dissolving methods on proteomic profiling of organoids. *Mol. Cell. Proteomics* **21**, 100181 (2022).
49. H. Yu, Y. Yang, L. Cao, J. Ji, J. Wu, Data from 'Dual roles of beta-arrestin 1 in mediating cell metabolism and proliferation in gastric cancer'. GSA for Human, NGDC. https://ngdc.cncb.ac.cn/gsa-human/browse/HRA002205. Deposited 2 April 2022.